Research Article Vol. 32, No. 27 / 30 Dec 2024 / Optics Express 48599
Optics EXPRESS

Spectral broadening of µJ-level pulses around 8 µm in a Germanium-based multi-pass scheme

FRANCESCO GUCCI,[1,†] ALESSANDRO BASERGA,[1,†] LUCA MORETTI,[1,2] DAVIDE GATTI,[1,2] MATTEO CORTI,[1] CRISTIAN MANZONI,[3] GIULIO CERULLO,[1] MARCO MARANGONI,[1,2] AND GUGLIELMO VESCO[1,2,*]

[1]*Dipartimento di Fisica, Politecnico di Milano, 20133 Milano, Italy*
[2]*IFN-CNR, Via Gaetano Previati 1/C, 23900 Lecco, Italy*
[3]*IFN-CNR, Leonardo da Vince, 32 Milano, Italy*
[†]These authors contributed equally to this work
[*]*guglielmo.vesco@polimi.it*

Abstract: A 2.6-fold spectral broadening of mid-infrared femtosecond µJ-level pulses has been achieved using an unfolded multi-pass configuration of germanium plates and zinc selenide lenses. This method maintains a throughput higher than 60% while preserving the spatial quality and the temporal duration of the input beam. Numerical simulations match the experimental results and show the potential to tailor the parameters of the cell to obtain different spectra.

1. Introduction

Nonlinear multi-pass cells (MPCs) have been a very successful tool in recent years to spectrally broaden and post-compress near-infrared (NIR) pulses [1]. They are based on self-phase modulation (SPM) in third- order nonlinear media that can be solid or gaseous depending on the pulse energy [2]. At every pass, the medium imparts a tiny amount of nonlinear phase to the circulating pulse that eventually results, after a large number of passes and proper dispersion control, in large B-integrals and broadening factors up to about 40 [3]. Importantly, this comes together with very high throughputs [4], average optical powers up to the kW level [5], high spatio-spectral homogeneity [6], and the possibility to reach the single-cycle regime upon suitable post-compression [7–9]. MPCs have been successfully implemented so far in the NIR region, mostly from Yb lasers with high average and peak power [10] and more recently from Tm-based lasers at 2 µm [11].

Nonlinear MPCs would be of great interest also in the mid-infrared (MIR) region, in the range from 5 to 12 µm, where a variety of linear and nonlinear spectroscopies call for high-energy broadband pulses. Examples of such experimental techniques are vibrationally resonant sum-frequency generation to explore surfaces and interfaces [12,13], high-harmonic generation from solid media to study band structures and electronic properties of materials [14–16], time-resolved IR and 2D IR spectroscopies to monitor chemical reactions by their characteristic molecular vibrational fingerprints [17–19], Fourier transform and photothermal infrared microscopies to map the chemical composition of biomedical samples such as cells and tissues [20,21]. Due to the absence of native sources of femtosecond laser pulses in the MIR, ultrashort MIR pulses are typically produced by difference-frequency generation (DFG) between pump and signal pulses in the NIR, where gain and bandwidth are traded off by group velocity matching conditions [22]. This trade-off is typically solved by the use of a short DFG crystal to attain the target bandwidth and by a high number of nonlinear amplification stages to boost the energy of the NIR pulses that are mixed for DFG [23–25]. This increases the system complexity to a level that is acceptable for fundamental science but it is unsatisfactory for applications, e.g., in the biomedical field.

#544183 https://doi.org/10.1364/OE.544183
Journal © 2024 Received 10 Oct 2024; revised 21 Nov 2024; accepted 23 Nov 2024; published 20 Dec 2024

Optics EXPRESS

An alternative more straightforward approach is to use a longer DFG crystal to achieve the desired MIR pulse energy [26,27], at the expense of its bandwidth, and to subsequently expand the optical bandwidth in a spectral broadening stage based on SPM. This approach has been pursued by single passes through bulk media, carefully balancing crystal length, input pulse energy, focusing conditions and central wavelength as a function of linear and nonlinear properties of the material chosen [28,29]. In general, however, single passes in bulk media result in a radially changing spectral content and in a degraded beam spatial quality [30,31]. This occurs also when cascaded quadratic processes are used to imprint SPM effects, with the additional constraint of a fine tuning of the phase mismatch between the interacting waves [27,32]. A completely different method to increase the MIR pulse energy and bandwidth is to start from high-energy laser sources at 2 µm [33,34]: in a long wavelength pumping scenario, thanks to much more favorable group-velocity matching conditions, interpulse DFG is indeed an effective way to generate ultrabroadband pulses in the MIR with efficiencies that can be higher than 1% [35]. As a downside, complexity and cost issues are here shifted to the laser source, due to the limited commercial availability of ultrafast Tm-, Ho- and Cr-based sources. In this paper we explore the feasibility to broaden MIR pulses at wavelengths from 7 to 8 µm in a multi-pass scheme. While previous numerical studies had investigated pulse compression based on spectral broadening at 3 and 6 µm in a MPC system [36], this is, to the best of our knowledge, the first experimental demonstration of a MPC approach in the MIR spectral range. We chose germanium (Ge) as a third-order nonlinear medium because of its ultrabroad transparency range, from 2 to 14 µm, its almost frequency independent positive dispersion across the entire range and its huge nonlinear refractive index [37–40], which is about three orders of magnitude higher than that of fused silica [1], allowing the energy threshold for spectral broadening to be reduced to the µJ level, even at long wavelengths. Rather than using a conventional MPC consisting of two reflecting mirrors [1], we preferred an unfolded variant where a sequence of Ge plates is alternated with zinc-selenide (ZnSe) lenses of short focal length, on the one hand to partially compensate for Ge dispersion along the cell and on the other hand to impart, thanks to the tight focusing, a sufficient nonlinear phase per pass with pulses of 1 µJ energy. After 6 passes we observe a broadening factor of 2.6 at 7.5 µm, together with a fully preserved spatial quality and a satisfactory throughput of 66%. Spectral broadening is also observed changing the central wavelength in the region from 6.9 µm to 8 µm, demonstrating the robustness of the system. The spectral shape at the cell output is smooth and very well reproduced by numerical simulations. Potential improvements of this first implementation are discussed with the help of simulations and literature.

2. Experimental setup and methods

2.1. Generation of MIR pulses

The narrowband MIR pulses to be spectrally broadened through the Ge-based unfolded MPC are generated by DFG between an Yb laser and the output of a non-collinear optical parametric amplifier (NOPA), as shown in Fig. 1 [41]. The system is powered by a regeneratively amplified femtosecond Yb:KGW laser (Carbide, Light Conversion), delivering 200-µJ, 230-fs pulses at 1.03 µm with a repetition rate of 25 kHz. The NOPA is pumped by the second harmonic (SH) of the Yb laser and seeded by the NIR part of a white light continuum (WLC). The former is generated in a 2-mm-thick β-barium borate (BBO) crystal (θ = 23.4°), the latter in a 10-mm-thick YAG plate. Parametric amplification takes place in a 3-mm-thick BBO crystal cut for type I phase matching (θ = 23.4°) with a non-collinear interaction angle of ~ 3° (external) and produces broadband pulses with center wavelength around 1.2 µm and energy of 350 nJ. These pulses are used as a signal for the collinear DFG stage, which is pumped by 90 µJ of the laser fundamental wave at 1.03 µm. The nonlinear interaction takes place in a 7-mm-thick lithium thiogallate (LGS) crystal cut for type II phase matching (θ = 90°, ϕ = 38.4°, Ascut Ltd) and generates µJ-level idler MIR pulses. The pump and signal FWHM beam diameters at the LGS position are 1500

Optics EXPRESS

μm and 880 μm respectively, whereas the generated MIR beam has a diameter of 470 μm. The second stage employs a strict collinear geometry to avoid angular dispersion of the idler pulses. The generated idler pulses are tunable in the spectral range between 6 and 9 μm and exhibit a FWHM spectral bandwidth ranging from 160 nm at 6.3 μm to 475 nm at 8.7 μm, as shown in Fig. 2. This significant increase in bandwidth upon tuning the idler towards longer wavelengths is due to the decreasing GVM between the signal and idler, resulting in a larger phase matching bandwidth [42]. The broadest spectra of MIR pulses are observed near 8.5 μm, where the signal and idler have the same group velocity.

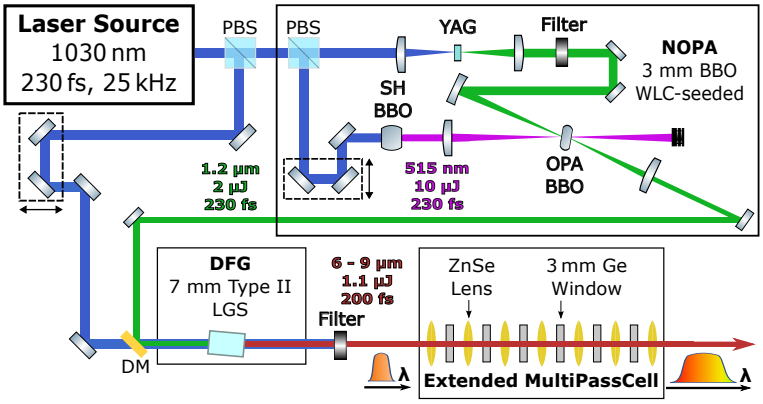

Fig. 1. Block diagram of the optical setup. Several opto-mechanical elements of the actual setup are not represented for the sake of clarity.

2.2. *Unfolded multi-pass cell*

The unfolded MPC is made of six 3-mm-thick AR-coated Ge plates alternated with seven zinc selenide (ZnSe) lenses (f = 40 mm, 2.4 mm thickness, from Thorlabs) placed at a confocal distance from one another. The Ge plates are positioned halfway between the lenses, where the beam diameter (FWHM) is calculated to be 350 μm, a value that corresponds in our experimental conditions to a nonlinear phase shift per pass not exceeding the threshold of 0.2 π for spatial distortions of the beam [1].

In this design, the positive group delay dispersion (GDD) of Ge is countered by the negative GDD of ZnSe between 6.5 μm and 9 μm, as shown in Fig. 2. This compensation limits temporal broadening of the pulse while propagating through the MPC, thereby maintaining an almost constant peak intensity across the Ge plates. Additionally, lenses allow for shorter focal lengths as compared to the concave mirrors typically used in conventional folded MPC. This results in smaller beam diameters and, consequently, greater intensities in the third-order nonlinear media even with low-energy pulses.

2.3. *Simulation of the spectral broadening*

To gain a better understanding of the non-linear broadening, we performed simulations of the pulse propagation through the MPC, using a custom-made Matlab script based on the split-step Fourier method that treats dispersion to all orders and SPM only in the time domain. The MIR pulse before the MPC is described in the frequency domain as:

$$\tilde{E}(\omega) = \tilde{E}_{TL}(\omega)e^{i\phi(\omega)} \tag{1}$$

where $\tilde{E}_{TL}(\omega)$ is the electric field of a transform-limited pulse evaluated from the experimental spectrum in absence of MPC, and $\phi(\omega)$ is the spectral phase caused by linear dispersion in the

Optics EXPRESS

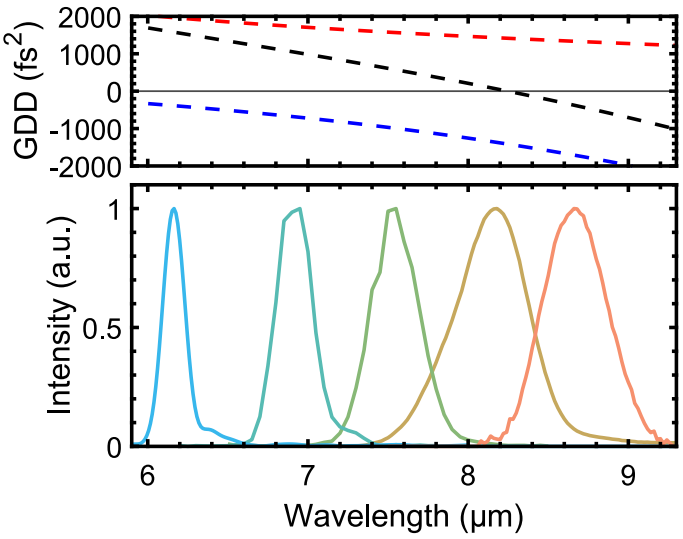

Fig. 2. On the top: GDDs introduced by a single pass through the cell elements: Ge (dashed red line), ZnSe (dashed blue line), and the combined total dispersion (dashed black line) On the bottom: different spectra produced by the MIR DFG stage.

optical elements that precede the MPC, namely LGS, ZnSe and Ge:

$$\phi(\omega) = k_{LGS}(\omega)d_{LGS} + k_{ZnSe}(\omega)d_{ZnSe} + k_{Ge}(\omega)d_{Ge} \tag{2}$$

In Eq. (2), $k_i(\omega)$ are extracted from the Sellmeier curves of the three media, $d_{ZnSe} = 4$ mm and $d_{Ge} = 1$ mm are the thicknesses of a collimating lens and of a Ge plate that filters out the pump and the signal after the DFG stage, respectively, while d_{LGS} is a free parameter that corresponds to the effective propagation length in LGS, which is remarkably shorter than the actual crystal thickness (equal to 7 mm) in a DFG process with high parametric gain. We extracted d_{LGS} by making the computed field $\tilde{E}(\omega)$ consistent with the experimental autocorrelation of the pulses before the MPC. This approach neglects the dispersion that the DFG process transfers with an opposite sign to the idler pulses in the presence of frequency chirped signal pulses, but this contribution is minimal as compared to that given by the highly dispersive LGS crystal at the adopted MIR wavelengths (GVD ≈ -2000 fs^2/mm at 7.5 μm). Furthermore, in the presence of initially chirped signal pulses, our approximation would only result in an over-(under-) estimation of the LGS effective length, without affecting the final $\tilde{E}(\omega)$.

Once $\tilde{E}(\omega)$ is known, the simulation provides the linear and nonlinear pulse evolution across a sequence of six 3-mm-thick Ge windows and a corresponding number of 2.4-mm thick ZnSe lenses. In the split-step method, we subdivide the Ge plates into slices of infinitesimal thickness. For each slice, we introduce the phase terms induced by the linear dispersion and by the nonlinear SPM. The former, is treated in the frequency domain as explained before, while the latter is computed in the time domain under a simple plane-wave approximation as:

$$\phi_{SPM} = -\frac{2\pi}{\lambda_0} n(I) d_{Ge} \tag{3}$$

where λ_0 is the central wavelength of the pulse and

$$n(I) = n_0 + n_2 I(t) \tag{4}$$

in which $I(t)$ is the time dependent intensity profile of the propagating pulse, n_0 is the refractive index at the central wavelength, and n_2 is the nonlinear refractive index. In our simulations we

Optics EXPRESS

considered $n_2 = 1 \cdot 10^{-17}$ m^2/W [37] because it provided the closest match to our experimental spectra, better than other values reported in the literature, such as $0.5 \cdot 10^{-17}$ m^2/W [38] and $2 \cdot 10^{-17}$ m^2/W [39]. The calculation of the linear and nonlinear dispersion is repeated six times, for every Ge plate, adding after each plate the linear dispersion contribution of the ZnSe lenses. In this way we get an insight into the spectral and temporal evolution of the pulses at each passage for different pulse energies, and we may eventually compare experimental and numerical spectra.

3. Results and discussion

To validate our approach, we first investigated the broadening through the MPC of pulses centered at 7.5 µm, in a regime of slight positive dispersion.

The top panel of Fig. 3 shows the measured and simulated broadened spectra (represented by the blue and red lines, respectively) alongside the original spectrum before broadening (represented by the black dashed line) for pulses centered at 7.5 µm. At the output of the MPC the pulses exhibit a broadening factor of 2.6 in the spectral FWHM, with an appreciable power throughput of 66% and a spectrum covering the range between 6.7 µm and 9 µm without any significant gaps or irregularities. The bottom panel of Fig. 3 displays the experimental autocorrelation of the pulses injected into the MPC together with those measured and simulated at its output. The FWHM of the autocorrelation of the input pulse centered at 7.5 µm is 366 fs, and that of the broadened

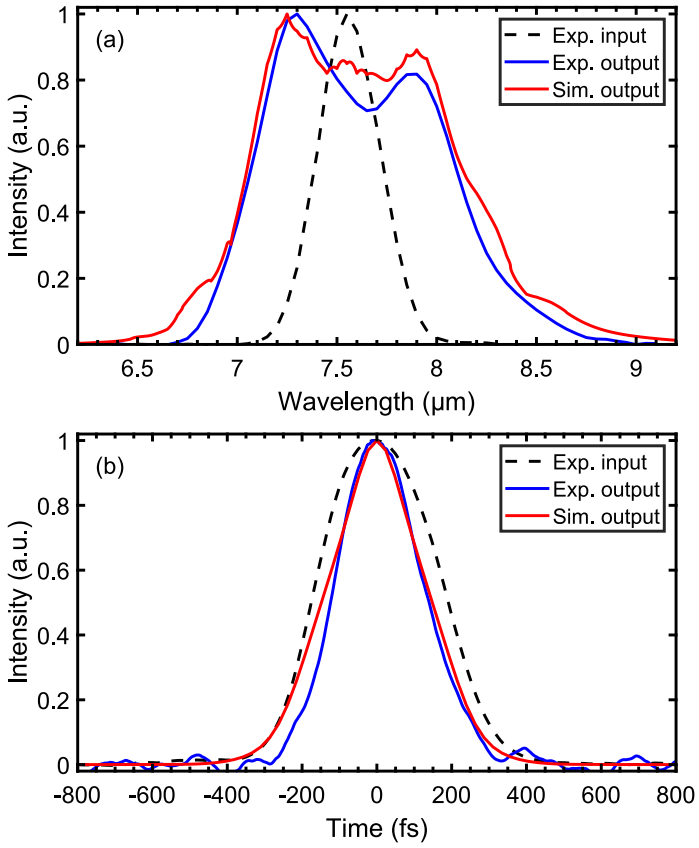

Fig. 3. (a) Input experimental spectrum (dashed line), experimental (blue) and simulated (red) output spectra for pulses center at 7.5 µm. (b) Corresponding autocorrelations.

Optics EXPRESS

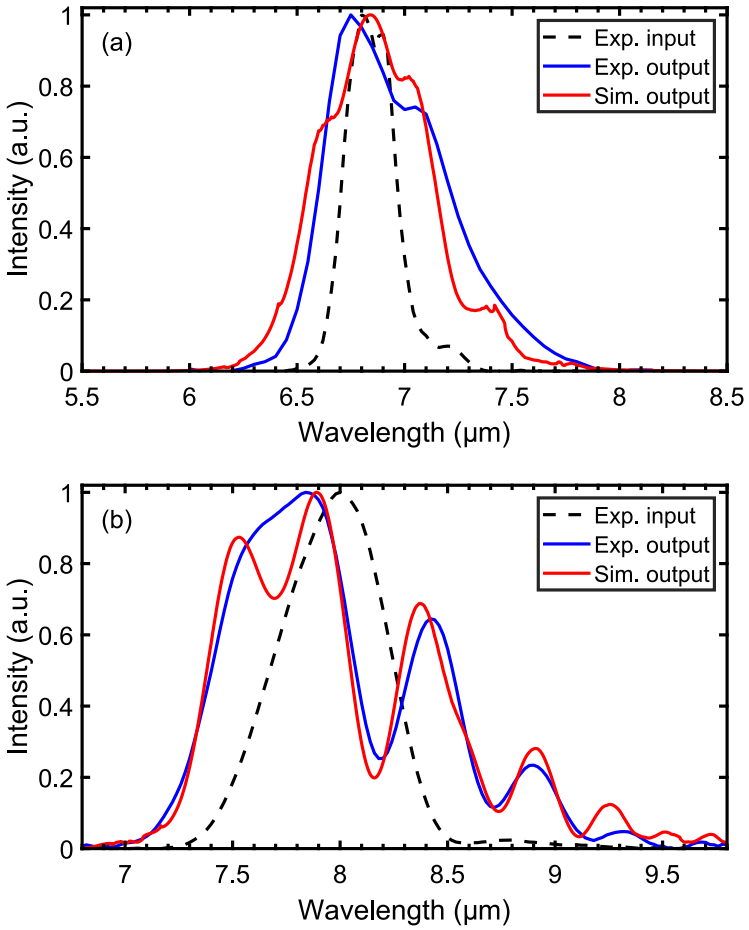

Fig. 4. Input (dashed), experimental (blue) and simulated (red) spectra for pulses center at 6.9 μm (top) and at 8 μm (bottom).

pulse is 264 fs, resulting in pulse durations of 259 fs and 186 fs, respectively. This shows that the pulse duration is only slightly altered by the MPC, indicating effective compensation of the Ge dispersion with that introduced by ZnSe. The output pulse is chirped, but further compression can be achieved using an additional post-compression stage. Overall, there is a good agreement between experiments and simulations for both spectral and temporal behavior.

Similar results were obtained using input pulses with different central wavelengths, as shown in Fig. 4. In particular, at 6.9 μm the FWHM bandwidth increases by a factor of 2.2, with spectra ranging from 6.2 to 7.9 μm, whereas at 8 μm the broadening is by 1.9 times, with an extension from 6.9 to 9.8 μm. The broadened spectrum obtained from pulses centered at 8 μm displays a peculiar modulated structure with decreasing peaks towards longer wavelengths, which is typical when the net linear dispersion tends to be zero under SPM [43].

Interestingly, the spectral broadening is achieved without significantly affecting the spatial beam quality, as demonstrated in Fig. 5, which compares the beam profiles before and after passage through the MPC. The top panels show the measured beam spot at the input (left) and output (right) of the MPC, while the bottom panels present the corresponding cross-sectional intensity profiles. The beam spot images reveal that the spatial distribution remains nearly

Optics EXPRESS

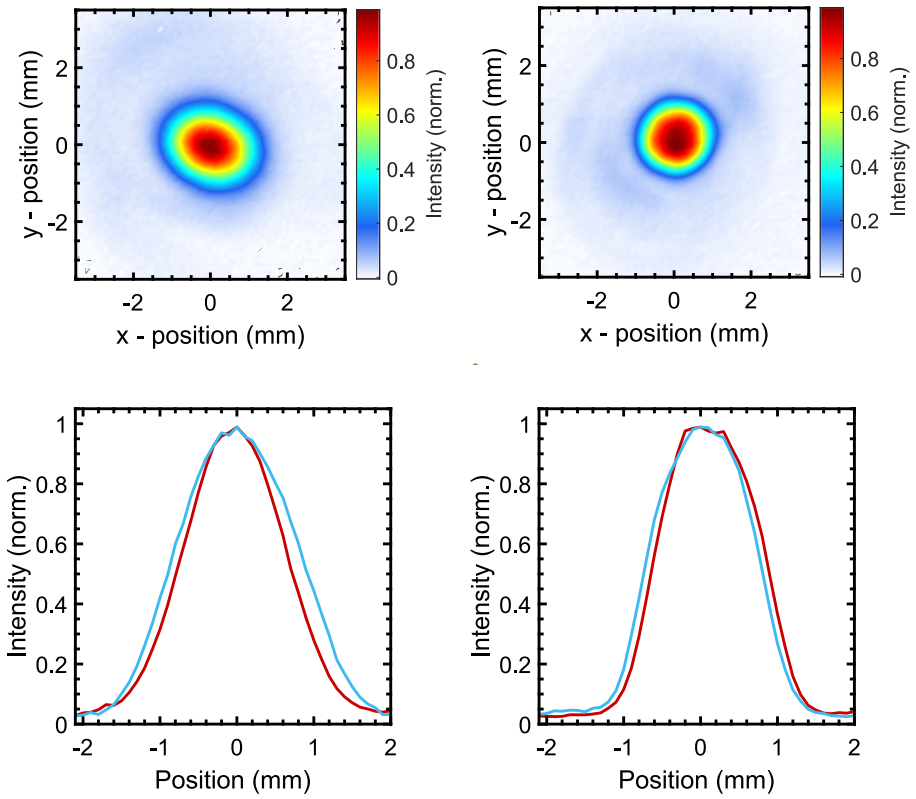

Fig. 5. (Top) Measured spot of input (left) and output (right) beam. (Bottom) Vertical (red) and horizontal (blue) cuts of the figures above.

unchanged after passage through the MPC, with both input and output beams maintaining a well-defined, symmetric Gaussian profile, as also highlighted by the comparison between the horizontal and vertical cross-sectional profiles, indicating that the spectral broadening process does not introduce significant distortions or degradation in beam quality, as it is typical of the MPC configuration.

Figure 6 presents the simulation results for increasing numbers of passes through the system for input pulses at 6.9, 7.5, and 8 µm. After one pass, the spectral broadening is negligible for pulses at 6.9 and 7.5 µm, while the central peak of pulses at 8 µm shows a slight narrowing, accompanied by the emergence of a small sideband at 8.4 µm. As the number of passes increases, significant broadening of the spectrum is observed for all three wavelengths. Notably, after four passes the broadening becomes appreciable, with the spectral features beginning to emerge: the broadened spectra obtained from the pulses centered at 6.9 and 7.5 µm display no gaps, whereas for pulses centered at 8 µm the central peak narrows and shifts to shorter wavelengths with sidebands appearing at longer wavelengths. The absence of saturation in the spectral broadening, even after six passes, suggests that increasing the number of passes could further enhance the broadening effect. The simulations show that, for input spectra centered at 7.5 and 8 µm, the optical bandwidth progressively increases until reaching a number of 24 passes, i.e. until the added nonlinear phase per pass becomes negligible due to the coating losses at the ZnSe and Ge interfaces. The spectral extension does not anyway exceed the 6-10 µm range, while the throughput drops to 20 %. Starting from spectra centered at 6.9 µm, there is instead no significant spectral gain beyond the adopted 6 passes, due to the net positive dispersion in the cell. To

Optics EXPRESS

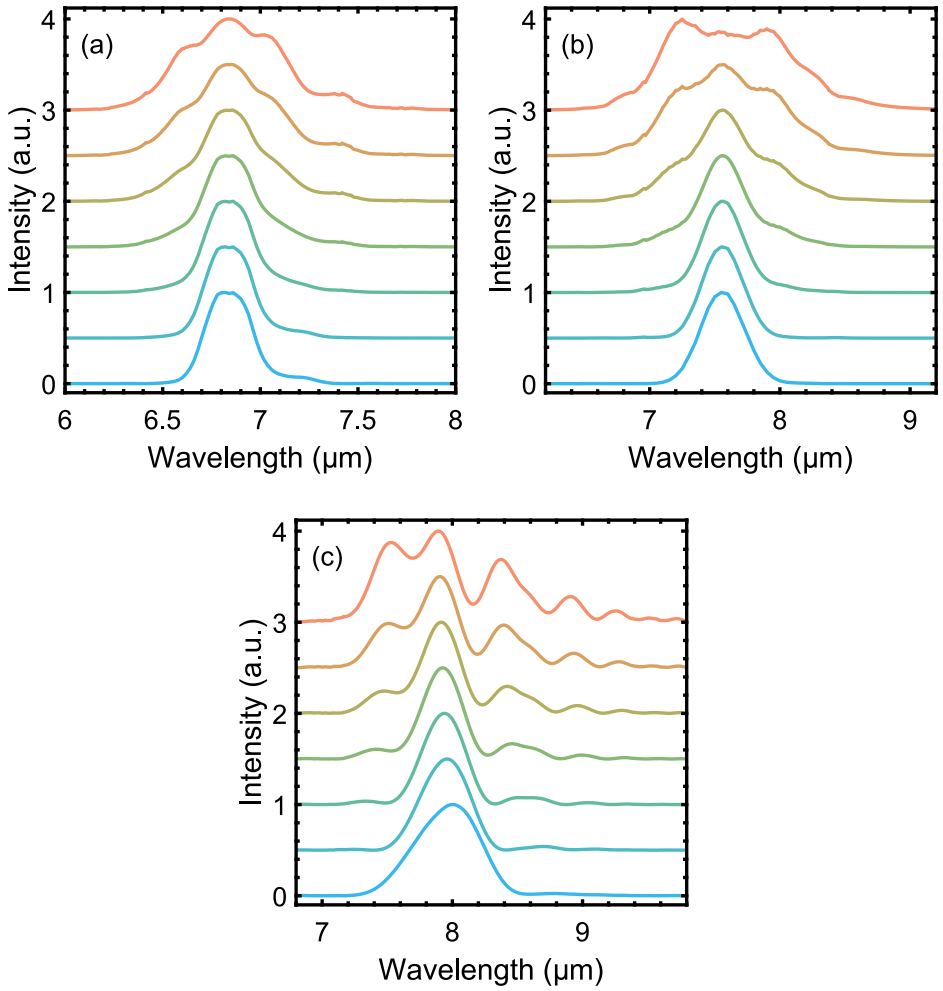

Fig. 6. Simulation of spectral broadening at increasing number of round trips with different pulses centered at 6.9 μm (a), 7.5 μm (b) and 8 μm (c), starting from the input spectrum at the bottom and going up to 6 passes on the top.

optimize the spectral broadening for a given number of passes, and thus for a given throughput, one might use Ge plates of increasing thickness throughout the cell or differentiate the position of Ge plates between each lens pair, choosing the beam-waist position (where the intensity is maximum) only for the last plates. This would lead indeed to a constant amount of nonlinear shift per pass despite the progressive pulse energy loss across the cell.

For pulses centered at 7.5 μm the dependence of spectral broadening on fluence was also investigated, by acquiring broadened spectra at different input pulse energies and comparing them against simulations. Figure 7 compares the experimental (left panel) and simulated (right panel) spectra obtained upon varying the input energy from 0.4 to 1.1 μJ. In the experimental results, as the input power increases, a progressive broadening of the spectral width is observed, with the broadest spectrum occurring at the highest energy of 1.1 μJ. The spectral profiles also show slight changes in shape, particularly at higher powers, where there is a small decrease in the intensity of the main peak, accompanied by the emergence and growth of two slightly higher

Optics EXPRESS

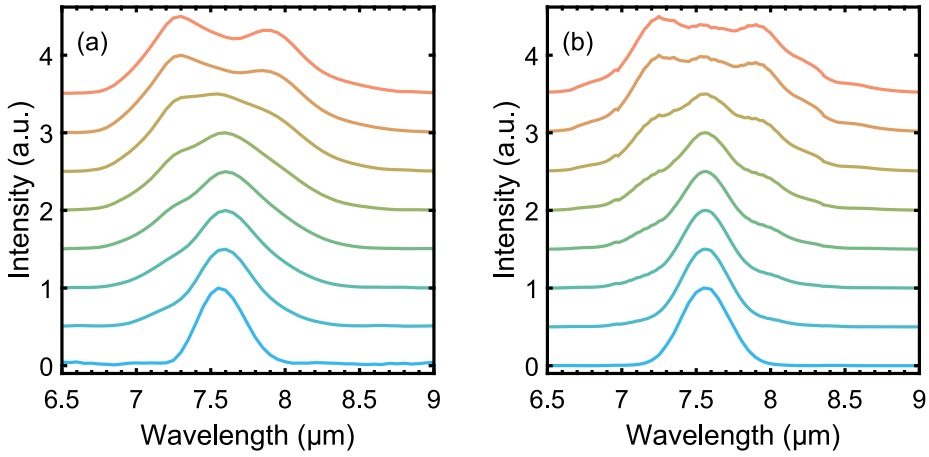

Fig. 7. Spectral broadening at different input energies, from bottom to top respectively of 0.16, 0.40, 0.52, 0.64, 0.76, 0.88, 1.01, and 1.04 μJ, experimental (left) and simulated (right). The spectra in both panels are represented using a gradient from cooler to warmer colors, corresponding to increasing input energies

additional peaks, consistent with the SPM features. The simulated spectra, in agreement with the experimental data, exhibit a consistent broadening trend with increasing input power. The simulations predict the emergence of additional spectral features and overall spectral broadening, which closely align with the experimental observations. However, some differences in the fine structure of the spectral profiles can be noted, particularly in the exact positioning and prominence of the additional peaks. Overall, the comparison between the experimental and simulated results demonstrates a good agreement, especially in terms of the general broadening behavior with increasing fluence. The differences observed in the finer spectral features may be attributed to experimental conditions not fully captured in the simulations, or simplifications in the modeling process.

While the general agreement between experimental and simulated results is reassuring, the application of our MPC method to higher pulse energies is subject to some constraints, particularly for wavelengths below 8 μm, where four-photon absorption may play a significant role. Based on the four-photon absorption coefficient of 0.01 cm^5/GW^3 at 6 μm reported in Ref. [38], a relatively low multiphoton absorption of 6% per plate is estimated in our experimental conditions (namely pulse energy of 1 μJ, pulse duration of about 250 fs and FWHM diameter around 350 μm). After 6 passes this corresponds to a 69% throughput that is consistent with our results, considering the good quality of the adopted anti-reflection coatings. At a doubled pulse energy, however, the single-pass transmission would drop to 72%, yielding an overall cell throughput of only 14% that might be detrimental for the applicability of the method. This deserves to be further investigated using either higher pulse energies or smaller focal spots that might be obtained with lenses with shorter focal length. As the wavelength exceeds 8 μm, constraints associated with four-photon absorption are no longer applicable, reducing the likelihood of encountering significant non-linear absorption issues. In fact, five-photon absorption mechanisms, which could potentially arise at these wavelengths, are less probable and, to the best of our knowledge, undocumented in the literature.

Optics EXPRESS

4. Conclusion

In this work we presented an extended multi-pass scheme for mid-infrared pulses based on germanium and zinc selenide, which achieves a 2.6 broadening factor in the 6 to 9 μm spectral range. The broadening is achieved with moderate energy (μJ level) femtosecond pulses, opening the possibility to use this system with high repetition rate lasers. The spatial quality of the laser beam is fully preserved by the multi-pass cell, despite the fact that the broadening is achieved through self-phase modulation in the germanium plates. Our simulations show the potential to tailor the broadening by scaling the power and/or increasing the number of passes inside the cell.

Funding. HORIZON EUROPE European Innovation Council (EIC-2021-PATHFINDEROPEN-01, 101047137); Ministero dell'Università e della Ricerca (PRIN 2022-ID 2022ZFFK58 (Project TROPIC).

Acknowledgements. We warmly thank Wolfgang Schweinberger and Alex Weigel for lending us the LGS crystal.

Disclosures. The authors declare no conflicts of interest.

Data availability. Data underlying the results presented in this paper are available in Ref. [44].

References

1. A. L. Viotti, M. Seidel, E. Escoto, *et al.*, "Multi-pass cells for post-compression of ultrashort laser pulses," Optica **9**(2), 197–216 (2022).
2. M. Hanna, F. Guichard, N. Daher, *et al.*, "Nonlinear optics in multipass cells," Laser Photon. Rev. **15**(12), 2100220 (2021).
3. P. Balla, A. B. Wahid, I. Sytcevich, *et al.*, "Postcompression of picosecond pulses into the few-cycle regime," Opt. Lett. **45**(9), 2572–2575 (2020).
4. S. Goncharov, K. Fritsch, and O. Pronin, "Few-cycle pulse compression and white light generation in cascaded multipass cells," Opt. Lett. **48**(1), 147–150 (2023).
5. C. Grebing, M. Müller, J. Buldt, *et al.*, "Kilowatt average-power compression of millijoule pulses in a gas-filled multi-pass cell," Opt. Lett. **45**(22), 6250–6253 (2020).
6. J. Schulte, T. Sartorius, J. Weitenberg, *et al.*, "Nonlinear pulse compression in a multi-pass cell," Opt. Lett. **41**(19), 4511–4514 (2016).
7. M. Müller, J. Buldt, H. Stark, *et al.*, "Multipass cell for high-power few-cycle compression," Opt. Lett. **46**(11), 2678–2681 (2021).
8. P. Rueda, F. Videla, T. Witting, *et al.*, "8 fs laser pulses from a compact gas-filled multi-pass cell," Opt. Express **29**(17), 27004–27013 (2021).
9. G. Barbiero, H. Wang, M. Grassl, *et al.*, "Efficient nonlinear compression of a thin-disk oscillator to 8.5 fs at 55w average power," Opt. Lett. **46**(21), 5304–5307 (2021).
10. C.-L. Tsai, F. Meyer, A. Omar, *et al.*, "Efficient nonlinear compression of a mode-locked thin-disk oscillator to 27 fs at 98w average power," Opt. Lett. **44**(17), 4115–4118 (2019).
11. P. Gierschke, C. Grebing, M. Abdelaal, *et al.*, "Nonlinear pulse compression to 51-w average power gw-class 35-fs pulses at 2-μm wavelength in a gas-filled multi-pass cell," Opt. Lett. **47**(14), 3511–3514 (2022).
12. L. J. Richter, "Vibrationally resolved sum-frequency generation with broad-bandwidth infrared pulses," Opt. Lett. **23**(20), 1594–1596 (1998).
13. Z. Heiner, L. Wang, V. Petrov, *et al.*, "Broadband vibrational sum-frequency generation spectrometer at 100 khz in the 950-1750 cm -1 spectral range utilizing a ligas2 optical parametric amplifier," Opt. Express **27**(11), 15289–15297 (2019).
14. M. Hohenleutner, F. Langer, O. Schubert, *et al.*, "Real-time observation of interfering crystal electrons in high-harmonic generation," Nature **523**(7562), 572–575 (2015).
15. G. Vampa, T. J. Hammond, M. Taucer, *et al.*, "Strong-field optoelectronics in solids," Nat. Photonics **12**(8), 465–468 (2018).
16. S. Ghimire and D. A. Reis, "High-harmonic generation from solids," Nat. Phys. **15**(1), 10–16 (2019).
17. A. Ghosh, J. S. Ostrander, and M. T. Zanni, "Spatially resolved two-dimensional infrared spectroscopy via wide-field microscopy," Chem. Rev. **117**(16), 10726–10759 (2017).
18. C. Poellmann, P. Steinleitner, U. Leierseder, *et al.*, "Resonant internal quantum transitions and femtosecond radiative decay of excitons in monolayer wse2," Nat. Mater. **14**(9), 889–893 (2015).
19. M. Först, R. Mankowsky, and A. Cavalleri, "Mode-selective control of the crystal lattice," Acc. Chem. Res. **48**(2), 380–387 (2015).
20. I. Pupeza, M. Huber, M. Trubetskov, *et al.*, "Field-resolved infrared spectroscopy of biological systems," Nature **577**(7788), 52–59 (2020).
21. T. Yuan, L. Riobo, F. Gasparin, *et al.*, "Phase-shifting optothermal microscopy enables live-cell mid-infrared hyperspectral imaging of large cell populations at high confluency," Sci. Adv. **10**(8), eadj7944 (2024).
22. C. Manzoni and G. Cerullo, "Design criteria for ultrafast optical parametric amplifiers," J. Opt. **18**(10), 103501 (2016).

Optics EXPRESS

23. B. W. Mayer, C. R. Phillips, L. Gallmann, *et al.*, "Mid-infrared pulse generation via achromatic quasi-phase-matched opcpa," Opt. Express **22**(17), 20798–20808 (2014).
24. H. Liang, P. Krogen, Z. Wang, *et al.*, "High-energy mid-infrared sub-cycle pulse synthesis from a parametric amplifier," Nat. Commun. **8**(1), 141 (2017).
25. R. Budriunas, K. Jurkus, M. Vengris, *et al.*, "Long seed, short pump: converting yb-doped laser radiation to multi-µj few-cycle pulses tunable through 2.5–15?µm," Opt. Express **30**(8), 13009–13023 (2022).
26. Z. Heiner, V. Petrov, and M. Mero, "Efficient, sub-4-cycle, 1-µm-pumped optical parametric amplifier at 10??µm based on baga4s7," Opt. Lett. **45**(20), 5692–5695 (2020).
27. M. Seidel, X. Xiao, S. A. Hussain, *et al.*, "Multi-watt, multi-octave, mid-infrared femtosecond source," Sci. Adv. **4**(4), eaaq1526 (2018).
28. F. Silva, D. Austin, A. Thai, *et al.*, "Multi-octave supercontinuum generation from mid-infrared filamentation in a bulk crystal," Nat. Commun. **3**(1), 807 (2012).
29. C. Schönfeld, A.-C. Heinrich, L. Feuerer, *et al.*, "Coherent generation and field-resolved detection of nonlinear χ^3 spectral broadening in the multi-thz regime, in *Conference on Lasers and Electro-Optics/Europe (CLEO/Europe 2023) and European Quantum Electronics Conference (EQEC 2023)*, (Optica Publishing Group, 2023), p. ee _5 _1.
30. M. Seidel, G. Arisholm, J. Brons, *et al.*, "All solid-state spectral broadening: an average and peak power scalable method for compression of ultrashort pulses," Opt. Express **24**(9), 9412–9428 (2016).
31. V. Shumakova, P. Malevich, S. Ališauskas, *et al.*, "Multi-millijoule few-cycle mid-infrared pulses through nonlinear self-compression in bulk," Nat. Commun. **7**(1), 12877 (2016).
32. B. Zhou and M. Bache, "Multiple-octave spanning high-energy mid-ir supercontinuum generation in bulk quadratic nonlinear crystals," APL Photonics **1**(5), 050802 (2016).
33. D. Sanchez, M. Hemmer, M. Baudisch, *et al.*, "7 µm, ultrafast, sub-millijoule-level mid-infrared optical parametric chirped pulse amplifier pumped at 2 µm," Optica **3**(2), 147–150 (2016).
34. C. Gaida, M. Gebhardt, T. Heuermann, *et al.*, "Watt-scale super-octave mid-infrared intrapulse difference frequency generation," Light Sci Appl **7**(1), 94 (2018).
35. L. von Grafenstein, M. Bock, D. Ueberschaer, *et al.*, "Multi-millijoule, few-cycle 5 µm opcpa at 1 khz repetition rate," Opt. Lett. **45**(21), 5998–6001 (2020).
36. D. Carlson, M. Tanksalvala, D. Morrill, *et al.*, "Nonlinear post-compression in multi-pass cells in the mid-ir region using bulk materials," Opt. Lett. **47**(20), 5289–5292 (2022).
37. M. Montesinos-Ballester, C. Lafforgue, J. Frigerio, *et al.*, "On-chip mid-infrared supercontinuum generation from 3 to 13 μm wavelength," ACS Photonics **7**(12), 3423–3429 (2020).
38. B.-U. Sohn, C. Monmeyran, L. C. Kimerling, *et al.*, "Kerr nonlinearity and multi-photon absorption in germanium at mid-infrared wavelengths," Appl. Phys. Lett. **111**(9), 091902 (2017).
39. L. Zhang, A. M. Agarwal, L. C. Kimerling, *et al.*, "Nonlinear group iv photonics based on silicon and germanium: from near-infrared to mid-infrared," Nanophotonics **3**(4-5), 247–268 (2014).
40. S. Serna, V. Vakarin, J.-M. Ramirez, *et al.*, "Nonlinear Properties of Ge-rich Si1-xGex Materials with Different Ge Concentrations," Sci. Rep. **7**(1), 14692 (2017).
41. A. Villa, A. M. Ross, R. Gotti, *et al.*, "Broadly tunable mid-infrared femtosecond pulses directly generated by an optical parametric amplifier," OSA Continuum **4**(11), 2837–2844 (2021).
42. G. Cerullo and S. De Silvestri, "Ultrafast optical parametric amplifiers," Rev. Sci. Instrum. **74**(1), 1–18 (2003).
43. C. Finot, F. Chaussard, and S. Boscolo, "Simple guidelines to predict self-phase modulation patterns," J. Opt. Soc. Am. B **35**(12), 3143–3152 (2018).
44. F. Gucci, A. Baserga, L. Moretti, *et al.*, "Spectral broadening of µJ-level pulses around 8 µm in a Germanium-based multi-pass scheme," 1 October 2024, https://zenodo.org/doi/10.5281/zenodo.13865522.